Equilibrium Folding of the Core Histones: the H3−H4 Tetramer Is Less Stable than the H2A−H2B Dimer†

Douglas D. Banks and Lisa M. Gloss*

School of Molecular Biosciences, Washington State University, Pullman, Washington 99164-4660

Received October 7, 2002; Revised Manuscript Received April 11, 2003

ABSTRACT: To compare the stability of structurally related dimers and to aid in understanding the thermodynamics of nucleosome assembly, the equilibrium stabilities of the recombinant wild-type H3−H4 tetramer and H2A−H2B dimer have been determined by guanidinium-induced denaturation, using fluorescence and circular dichroism spectroscopies. The unfolding of the tetramer and dimer are highly reversible. The unfolding of the H2A−H2B dimer is a two-state process, with no detected equilibrium intermediates. The H3−H4 tetramer is unstable at moderate ionic strengths (μ ~0.2 M). TMAO (trimethylamine-*N*-oxide) was used to stabilize the tetramer; the stability of the H2A−H2B dimer was determined under the same solvent conditions. The equilibrium unfolding of H3−H4 was best described by a three-state mechanism, with well-folded H3−H4 dimers as a populated intermediate. When compared to H2A−H2B, the H3−H3 tetramer interface and the H3−H4 histone fold are strikingly less stable. The free energy of unfolding, in the absence of denaturant, for the H3−H4 and H2A−H2B dimers are 12.4 and 21.0 kcal mol^{-1}, respectively, in 1 M TMAO. It is postulated that the difference in stability between the histone dimers, which contain the same fold, is the result of unfavorable tertiary interactions, most likely the partial to complete burial of three salt bridges and burial of a charged hydrogen bond. Given the conservation of these buried interactions in histones from yeast to mammals, it is speculated that the H3−H4 tetramer has evolved to be unstable, and this instability may relate to its role in nucleosome dynamics.

The protein folding code, often termed the second half of the genetic code, describes not only the stability and structure of the native state of a protein but the mechanism for its rapid and efficient conversion from an unfolded, random coil to its native state. Deciphering the protein folding code, with its inherent plasticity and redundancy, is incomplete. Efforts to predict structure from sequence have improved significantly in the past decade but are still imperfect (*1*, *2*). The ability to estimate protein stability or folding mechanism from sequence alone is very limited. Even with the information of a three-dimensional structure model, understanding the relationships between stability and sequence often requires hindsight from experimental measurements of stability and mutational studies.

Comparisons of the stability and folding mechanisms of homologous proteins, with similar structures but varied sequences, will help elucidate the redundancies in the protein folding code, including ramifications for effects on protein stability. Such studies have been reported on a number of monomeric systems from mesophilic organisms (for review, ref *3*) as opposed to the comparison of mesophilic and thermophilic proteins where interpretation is complicated by evolutionary adaptations to altered environmental conditions. To date, the stability of only a few homologous oligomeric systems have been examined. In dimeric systems, the protein folding properties are encoded by not one, but two polypeptide chains. Examples that have been studied include ketosteroid isomerase from two bacterial species (*4*, *5*) and glutathione transferases from different subfamilies (*6*−*8*).

In the comparisons of homologous proteins, for many structures, despite significantly altered stabilities, similar kinetic folding landscapes are observed. Global features, such as two-state versus multi-state kinetics and parallel pathways or sequential pathways, are generally conserved, although the details of precise structures in the transition state and intermediates may vary, for example, in the case of the Ig-binding proteins L and G (*9*, *10*). These data may suggest that backbone structure—or secondary structure propensities—predominate in determining folding pathways. This hypothesis is supported by studies in the colicin binding immunity proteins, Im7 and Im9; the more stable Im9 folds by a two-state mechanism, but the higher helical propensity of a helical segment of Im7 results in the population of a transient kinetic intermediate (*11*). In contrast, side chain interactions may contribute more significantly to the details of structural stability. This paper extends these examinations of the protein folding code to the histone fold motif, as found in the core histones of the eukaryotic nucleosome, by comparing the stability of the heterotetramer, $(H3-H4)_2$, to that of the structurally related heterodimer, H2A−H2B.

The nucleosome core particle, the elemental subunit in the hierarchy of compaction of chromatin, is composed of an octamer of two copies each of four basic histone proteins

†This work was supported by grants to L.M.G. from the American Cancer Society (RPG-00-085-01-GMC) and the National Science Foundation (MCB-9983831). D.D.B. was partially supported by an NIH Biotechnology training grant (GM08336-13).

* To whom correspondence should be addressed. Phone (509) 335-5859. E-mail: lmgloss@wsu.edu.

10.1021/bi026957r CCC: $25.00 © 2003 American Chemical Society
Published on Web 05/14/2003

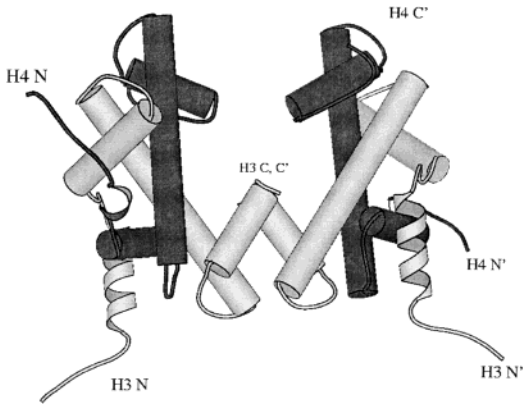

FIGURE 1: Ribbon structure of the histone fold and the dimer−dimer interface of the H3−H4 tetramer. The H3 monomers, from residues 38−135 of 135 total, are shown in the lighter gray; the darker colored H4 monomers encompass residues 20−102 of 102 total residues. The helices of the canonical histone fold are represented by cylinders. The figure was rendered from the coordinates of the tetramer in the core nucleosome (*12*), using Molscript v2.1 (*64*).

around which DNA is wrapped (*12*). The histone fold motif is the central architecture of the four core histone proteins; the motif contains a long central α helix, flanked on either end by β loops connecting to shorter α helices (*12, 13*). Histones H2A and H2B heterodimerize, as do histones H3 and H4, in a head to tail fashion known as the handshake motif (*13, 14*). The tetramer interface between two H3−H4 dimers is a four-helix bundle formed from the H3 C-termini (Figure 1). The histone fold dimerization motif is an important mediator of oligomerization in a variety of protein−DNA complexes. Sequence comparisons have suggested the motif is encoded in a number of DNA-binding proteins (*15, 16*); structural studies have shown that four of the TAFs (TATA-binding-protein-associated factors) of the TFIID transcription complex contain the canonical handshake motif (*17, 18*).

The sequence of a given histone is highly conserved from yeast to mammals, but there is minimal sequence identity, 4−6%, found between the histone proteins (*14*). However, the peptide backbones of the four histone monomers overlay with RMS deviations of 1.5−2.5 Å, demonstrating the high degree of structural conservation. Given this disparity between sequence and structural identity, the core histones provide an excellent model system for investigation of the redundancies of the protein folding code. A great deal of attention has focused on residues of the histones that are important for interaction with DNA and/or are posttranslationally modified (for review, see refs *19* and *20*). Comparatively few analyses have focused on the residues that are important for the protein stability of the histones; such residues may have an impact on the biological function of histones by determining their stability.

The folding reactions of the individual histones, in the context of their homotypic self-association interactions, were well-characterized by Isenberg (for review, see ref *21*). D'Anna and Isenberg also determined the dissociation constants for the heterotypic histone complexes from continuous variation curves monitored by fluorescence (FL) and circular dichroism (CD) (*22*). Their results indicated that the stabilities of the H3−H4 tetramer and H2A−H2B dimer were −28 and −8 kcal (mol oligomer)$^{-1}$, respectively (*23*). When compared on a per monomer basis, the ΔG for the H3−H4 association was still nearly double that for H2A−H2B (−7 and −4 kcal mol^{-1}, respectively). These free energy differences represent the stability difference between the weakly associated homotypic oligomers and the more stable, heterotypic assemblies observed in the nucleosome.

Thermal denaturation, using circular dichroism and differential scanning calorimetry (DSC), has also been used to determine the stability of the histone oligomers, relative to thermally unfolded monomers (*24*−*26*). However, the thermal unfolding of the H3−H4 tetramer was irreversible, and comparisons could only be made between the H2A−H2B dimer and the H3−H4 dimer populated at pH values below ~5. Across the various conditions of pH and ionic strength employed, the unfolding of the H2A−H2B dimer exhibited higher values of $\Delta H°$, $\Delta S°$, and ΔC_p than did the H3−H4 dimer. However, the values of T_M and $T°$, the midpoint of thermal unfolding transition and the temperature at which the $\Delta G°$ is zero, respectively, were higher for the H3−H4 dimer ($T_M \neq T°$ for a dimeric system). Using the value of ΔC_p and the DSC data, an extrapolation of the stability can be made to physiological temperatures. In similar solvent conditions (pH 5−5.5 and 40−50 mM salt) and 25 °C (the temperature used in this report), the H3−H4 dimer was slightly more stable than the H2A−H2B dimer, by ~0.3 kcal mol^{-1}, <10% of the total stability of H3−H4.

In the present study, we have determined the stabilities of the H3−H4 tetramer and the H2A−H2B dimer under identical conditions by GdnHCl-induced denaturation, monitoring far-UV CD and intrinsic Tyr FL. In comparison to previous reports, we have used recombinant histone proteins, produced in *Escherichia coli* (*27*). This histone source has the advantage, over chicken erythrocyte (*24, 25*) and calf thymus histones (*22*) used previously, of homogeneity with respect to a lack of posttranslational modifications. GdnHCl denaturation studies have an advantage over thermal studies by permitting determination of free energies at physiological temperatures, without ΔC_P-dependent extrapolations.

MATERIALS AND METHODS

Materials. Ultrapure guanidine hydrochloride was purchased from ICN Biomedicals (Costa Mesa, CA). TMAO[1] from Sigma (St. Louis, MO) was dissolved in H_2O and deionized in batch mode with AG 11A8 mixed-bed resin (BioRad, Richmond, CA). The concentration of TMAO was determined by refractive index as described elsewhere (*28*). Primary polyclonal antibodies to H3 (raised against the unacetylated N-terminal tail) and H4 (raised against full-length calf thymus H4) and HRP-conjugated secondary antibody were from Upstate Biotechnologies (Lake Placid, NY). Western blots were probed using the SuperSignal chemiluminescent substrate kit from Pierce (Rockford, IL).

[1] Abbreviations: β-ME, 2-mercaptoethanol; ASA, solvent accessible surface area; CD, circular dichroism; C_M, the denaturant concentration at which the apparent fraction of unfolded monomer constitutes 50% of the population; ΔASA, change in solvent accessible surface area between the associated and/or folded species and the dissociated and/or unfolded species; F_{app}, apparent fraction of unfolded monomer; FL, fluorescence; GdnHCl, guanidine hydrochloride; KPi, potassium phosphate, pH 7.2; MRE, mean residue ellipticity; SEC, size-exclusion chromatography; SF, stopped-flow; SVD, singular value decomposition; TMAO, trimethylamine-*N*-oxide.

Methods. *Production of Recombinant Histone Oligomers.* Recombinant histones were overexpressed in *E. coli* and purified as described elsewhere (*27*, *29*). The isolated H2A and H2B monomers in 10 mM HCl were reconstituted to the native heterodimer as described elsewhere (*29*). Reconstitution from acid-unfolded monomers was not successful with the H3−H4 tetramer; instead, monomers unfolded in 8 M GdnHCl were mixed and refolded by rapid dilution of the denaturant to concentrations less than 0.8 M. The folded tetramer was then dialyzed to remove the remaining GdnHCl and concentrated. The buffers used in the purification, storage, and experiments with H3 contained 1−5 mM β-ME to prevent H3−H3 disulfide cross-links between the wild-type Cys110 residues. The absence of such a cross-link was demonstrated by SDS−PAGE using loading buffers without reducing agent; no H3−H3 cross-linked species were observed. Extinction coefficients of 10 200 M^{-1} cm^{-1} and 19 300 M^{-1} cm^{-1}, respectively, were determined for the H2A−H2B dimer and H3−H4 tetramer by the method of Gill and von Hippel (*30*).

Analysis of Oligomeric Structure. HPLC size-exclusion chromatography, cross-linking experiments, and the equilibrium folding studies were performed in buffered solutions containing 200 mM KCl, 20 mM potassium phosphate, pH 7.2, 1 mM EDTA, 3 mM β-ME. To determine the native molecular weight of the histone oligomers, the proteins were chromatographed at room temperature on both a TosoHaas TSK G-3000SW column and a Phenomenex BioSep-SEC-S 3000 column. A Dawn EOS static light-scattering detector (Wyatt Technologies, Santa Barbara, CA) was coupled to the TSK column. Elution of the H2A−H2B dimer and the H3−H4 tetramer were compared to the elution of standards: bovine serum albumin, ovalbumin, chymotrypsinogen, and ribonuclease A.

To verify a heterotypic assembly of the H3−H4 tetramer, ~4 μM tetramer was cross-linked with glutaraldehyde. The cross-linking reactions were incubated with 0.002% glutaraldehyde for 1 h at 25 °C. The reactions were then precipitated with 10% trichloroacetic acid and electrophoresed on a 12% SDS−polyacrylamide gel. The species present in the cross-linked band were identified by Western blots. The proteins were transferred to a nitrocellulose membrane and probed as described in the literature from Upstate Biotechnology with antibodies specific to either H3 or H4. The blot was visualized using enhanced chemiluminescence as described in the Pierce protocols included in the SuperSignal kit.

GdnHCl Equilibrium Unfolding Titrations. All of the experiments were performed at 25 °C. CD data were collected on an AVIV 202SF spectrophotometer; FL data were collected on an AVIV Model ATF-105/305 differential/ratio spectrofluorometer. Both instruments were interfaced with Hamilton Model 500 automated titrators. CD titration data were monitored at 222 or 224 nm (in the presence of TMAO) or by collecting spectra from 260−220 nm at each GdnHCl concentration and analyzing the data using singular value decomposition (*31*). FL titration data were collected with an excitation wavelength of 280 nm and emission wavelength of 305−306 nm. In the automated titrations, equilibration times of 2−3 min were used and were significantly longer than times required for the complete folding and unfolding kinetics observed for the tetramer and dimer. Generally, titrations were performed by starting with folded protein in the cuvette and titrating with a stock of unfolded protein in GdnHCl at the same monomer concentration. Reversibility was assessed by performing titrations with GdnHCl unfolded protein in the cuvette and titrating with a stock of folded protein.

Stopped-Flow Unfolding Kinetics. Stopped-flow kinetics were monitored using an AVIV Instruments stopped-flow tower interfaced with the AVIV 202SF CD spectrometer. For SF−CD and SF−FL data, ~35 and 20 shots, respectively, were averaged for each kinetic trace to improve the signal-to-noise ratio of the data. SF−CD data were collected at 222 nm. SF−FL data, with excitation at 280 nm, were collected by monitoring the signal at 90° to the incoming light, after a 295 nm cutoff filter. The dead-time of the stopped flow instrument was ~5 ms, with a push velocity of 2 mL/s.

Data Analysis. Equilibrium unfolding transitions were globally fitted using the data analysis program, Savuka 5.1 (*32*−*34*). The errors of the fits were determined from rigorous analyses of the error surfaces of the fits (*35*). The models employed the common linear extrapolation between the free energy of unfolding, $\Delta G°$, and the denaturant concentration (*36*, *37*):

$$\Delta G = \Delta G(H_2O) - m[\text{GdnHCl}] \quad (1)$$

where $\Delta G°$ (H_2O) represents the free energy of unfolding in the absence of denaturant, and m reflects the sensitivity of the transition to the [denaturant]. Kinetic data were fit to a series of exponentials; local fits for each kinetic trace were fit using Kaleidagraph 3.5 (Synergy Software) or globally with linked relaxation times using Savuka 5.1.

Calculation of Accessible Surface Area. The solvent accessible surface area of the histone oligomers were calculated from the coordinates of the X-ray crystal structure of the core nucleosome (*12*), using the program ACCESS (*38*). Default values were used for probe radius (1.4 Å), slice width (0.25 Å), and atomic radii. Models for the unfolded monomers were generated using Insight II (Biosym Technologies, San Diego, CA), as described elsewhere (*39*), using β-sheet extended dihedral angles. This model was then submitted to ACCESS to calculate the extended, unfolded solvent accessible surface area. The composition of the surface area was dissected into polar (O and N) and nonpolar (C and S) atoms. Given the small number of S atoms in the histone monomers, their classification as polar or nonpolar had no significant effect on the results of parsing of the surfaces into polar and nonpolar content.

RESULTS

Characterization of the Histone Oligomers. The oligomeric states of the reconstituted histones were examined by HPLC size-exclusion chromatography (SEC), static light-scattering, and glutaraldehyde cross-linking. All of the data were consistent with dimeric H2A−H2B and a predominance of tetrameric H3−H4. Analytical velocity sedimentation ultracentrifugation results (L. Randall and L. M. Gloss, unpublished data) also supported the reconstitution to the appropriate oligomeric states.

The HPLC−SEC elution peak for the tetramer was much broader than for the H2A−H2B dimer, suggesting an equi-

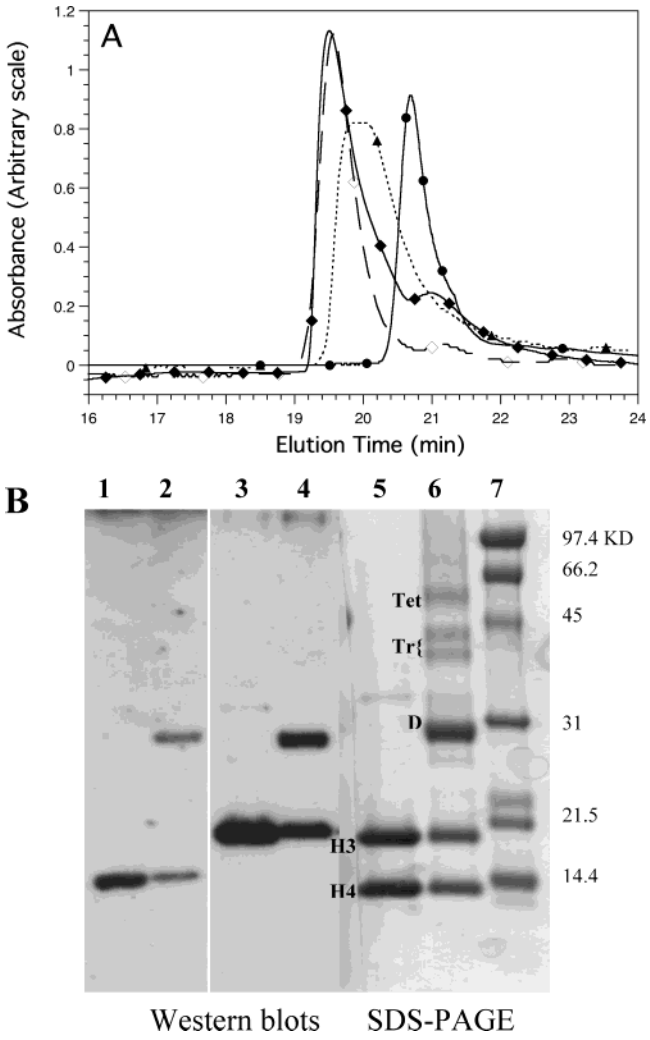

FIGURE 2: (A) HPLC size-exclusion chromatography of the core histones. The proteins were chromatographed on a BioSep-SEC-S 3000 column, equilibrated at room temperature in buffer with the cosolute concentration listed below and 20 mM potassium phosphate, pH 7.2, 1 mM EDTA, 3 mM β-ME, with detection at 280 nm. H2A−H2B, in 200 mM KCl, injected at 38 μM dimer, solid line, ●; H3−H4, in 200 mM KCl, injected at 21 μM tetramer, dotted line, ▲; H3−H4 in 1.5 M KCl, injected at 21 μM tetramer, dashed line, ◇; and H3−H4 tetramer in 1 M TMAO, injected at 12 μM tetramer, solid line, ◆. (B) Confirmation of the heterotypic association of the H3−H4 tetramer by cross-linking. 12% SDS−polyacrylamide gel stained with Coomassie Blue (lanes 5−7). Western blots of the cross-linked proteins were performed using anti-H4 (lanes 1 and 2), anti-H3 (lanes 3 and 4). Lanes 1, 3, and 5: H3−H4 tetramer not subjected to cross-linking. Lanes 2, 4, and 6: glutaraldehyde cross-linked H3−H4 tetramer. Lane 7: molecular weight standards. Labels in lane 6: Tet, tetrameric cross-linked H3−H4; Tr, cross-linked trimers comprised of H3 and H4; D, cross-linked H3−H4 dimer. Conditions: 200 mM KCl, 20 mM potassium phosphate, pH 7.2, 1 mM EDTA, 3 mM β-ME.

librium between a fully assembled tetramer and partially dissociated H3−H4 dimers (Figure 2A). Chromatography in the presence of 1.5 M KCl or 1 M TMAO (stabilizing osmolyte discussed below) resulted in much sharper elution peaks and a shorter elution time; these data are consistent with cosolute shifting the equilibrium to the more fully assembled H3−H4 tetrameric state. However, the folding equilibria could not be measured in 1.5 M KCl because of the tendency of H3−H4 to aggregate at high salt concentrations (*40*). TMAO did not appear to promote histone aggregation.

The proper heterodimeric association of H3 and H4 was verified by glutaraldehyde cross-linking. The cross-linked products were analyzed by SDS−polyacrylamide gel electrophoresis and Western blot analysis (Figure 2B). The major cross-linked species migrated on SDS−PAGE at the molecular weight of a dimer. Trimeric and tetrameric species were also observed in patterns very similar to those published elsewhere for dimethyl suberimidate cross-linking of H3−H4 histones (*41*). Western blot analysis confirmed that the dimeric species contained both H3 and H4 polypeptides. The higher order cross-linked species were not detected in the Western blot. This may be the result of their lower abundance and/or increased cross-links altering the epitopes, particularly for the anti-H3-tail antibody.

H2A and H2B could also be cross-linked to a dimeric state (data not shown). Western blots were not performed to confirm the heterotypic association of the cross-linked species. However, the altered SDS−PAGE migration of cross-linked dimers with combinations of full-length and N-terminal tail truncated H2A and H2B monomers demonstrated that both H2A and H2B monomers were present in the cross-linked species (B. J. Placek and L. M. Gloss, unpublished data).

The far-UV CD spectra of the reconstituted, recombinant histone oligomers are typical for α-helical proteins, with minima at 208 and 222 nm (data not shown). The ellipticity at 222−224 nm is sensitive to the unfolding of the secondary structure of the histones (i.e., Figures 3 and 4). The data presented in Figure 3A are normalized to mean residue ellipticity, correcting for the differing number of residues between the H2A−H2B and the H3−H4 oligomers. On a per residue basis, the dimer is more helical than the tetramer, as evidenced by the greater ellipticity of the dimer. A similar result was observed in previously published molar ellipticity CD data at the same ionic strength as the data in shown in Figure 3A (*26*).

Unfolding of the Histone Oligomers. The denaturant-induced unfolding transitions of H2A−H2B are highly reversible, with respect to both urea (*29*) and guanidine hydrochloride (GdnHCl), as shown in this report. However, reproducibly high reversibility could only be observed for the H3−H4 tetramer unfolded by GdnHCl. The unfolding transitions of the dimer and tetramer at equal monomer concentrations, monitored by CD at 222 nm, are shown in Figure 3A. The transitions are sigmoidal, with pre- and post-transition baselines. However, for the tetramer, the native baseline is relatively short and poorly determined.

Global fitting of H2A−H2B CD unfolding data at 2, 5, and 10 μM dimer yielded a free energy of unfolding in the absence of GdnHCl, $\Delta G°$ (H_2O), of 17 ± 1 kcal mol^{-1} at a standard state of 1 M dimer and a *m* value of 6.4 ± 0.6 kcal mol^{-1} M^{-1}. The *m* value describes the sensitivity of the transition to the denaturant concentration (eq 1). This parameter reflects the cooperativity of the unfolding, and in two-state unfolding systems, is usually proportional to the change in solvent accessible surface area exposed in the native and unfolded ensembles, ΔASA (*39*). The H3−H4 data shown in Figure 3 could not be reliably fit because of the very limited native baseline region. However, two observations can be made from the CD data shown in Figure 3A: (1) H3−H4 is less stable than H2A−H2B, requiring lower concentrations of denaturant to induce unfolding and

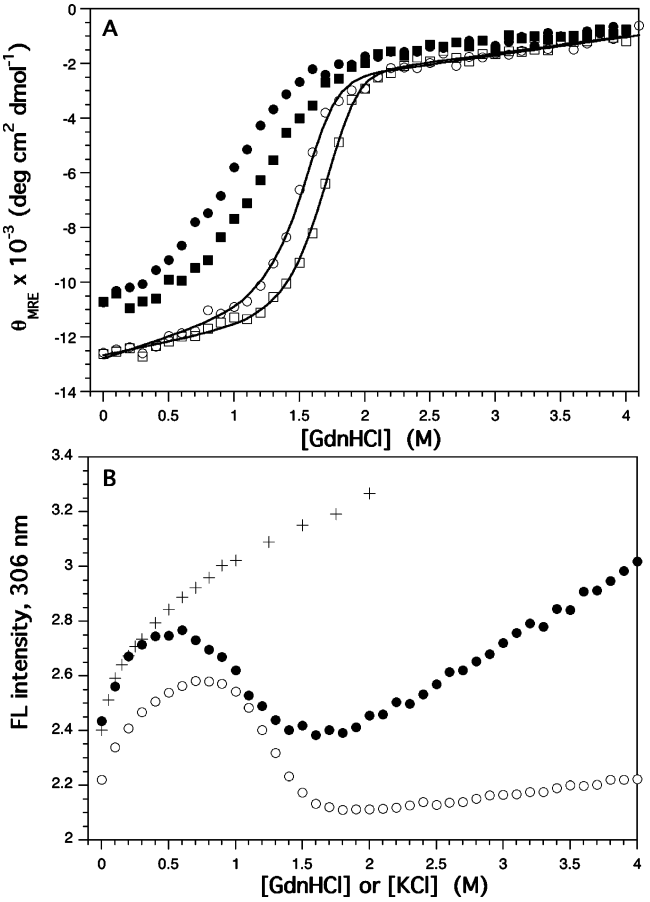

FIGURE 3: Representative GdnHCl-induced unfolding transitions of the histone oligomers in the absence of TMAO. (A) The far-UV CD ellipticity values are presented as mean residue ellipticity at 222 nm. H3−H4 tetramer at 1 (●) and 5 μM (■) tetramer; H2A−H2B dimer at 2 μM (○) and 10 μM (□) dimer. The solid lines represent the global fit of the H2A−H2B data to a dimeric, two-state equilibrium unfolding model. (B) Unfolding transitions of 1 μM H3−H4 tetramer (●) and 0.5 μM H2A−H2B dimer (○) monitored by Tyr FL, 306 nm. The FL of H3−H4 tetramer as a function of [KCl] is also shown (+). Conditions: 20 mM potassium phosphate, pH 7.2, 1 mM EDTA, 3 mM β-ME, and 200 mM KCl, at 25 °C.

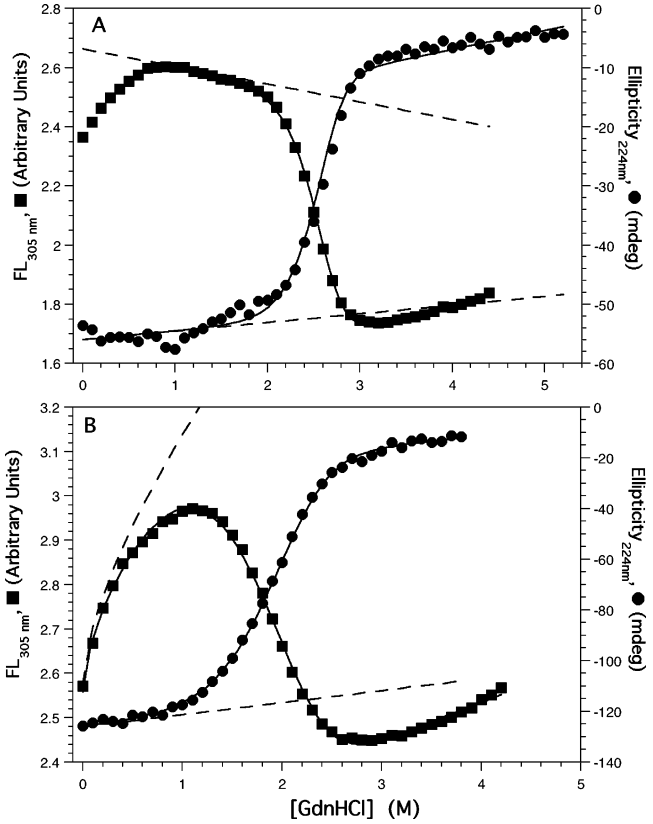

FIGURE 4: Representative GdnHCl-induced unfolding transitions of the histone oligomers in 1 M TMAO. FL intensity at 305 nm, ■, and CD ellipticity at 224 nm, ●. The lines represent the global fits of the data. The fitted native baselines are represented by dashed lines; for clarity, the well-defined unfolded baselines are not shown. (A) H2A−H2B dimer at 2 μM dimer, globally fitted to a two-state dimeric model. (B) H3−H4 tetramer at 2 μM tetramer, globally fitted to a three-state tetramer−dimer unfolded model. The native baseline was fitted to the function $Y_i = Y_{N,0} + S_N[\text{GdnHCl}]^n$, where $Y_{N,0}$ and S_N represent the intercept in the absence of GdnHCl and the slope of the baseline, respectively. This equation was chosen because it described well the salt-dependent increase in FL seen with KCl (Figure 2, inset). The exponent, n, fit to values of 0.45−0.48 for all FL data sets collected at several tetramer concentrations. Conditions are described in the legend of Figure 3.

(2) the unfolding transition of H3−H4 is less steep and less cooperative than that of the H2A−H2B dimer.

Unfolding transitions were also monitored by intrinsic Tyr FL (Figures 3B and 4), which served as a probe of the unfolding of the tertiary and quaternary structure of the core histones. The H3 and H4 monomers contain three and four Tyr residues, respectively. The H2A and H2B monomers contain three and five Tyr residues, respectively. The pre-transition baselines were very steep and curved for both the H2A−H2B and the H3−H4 oligomers, as shown in Figure 3B. This is in contrast to the linear, shallow, folded FL baseline observed for the urea-induced unfolding of the H2A−H2B dimer (*29*). The increase in the FL signal between 0 and ∼0.5 M GdnHCl could be the result of an unfolding transition or the effect of increased chloride salt on local structure around the Tyr residues that are partially solvent-exposed. Three pieces of data suggest that the latter explanation is the predominant cause of the FL changes in low [GdnHCl]. First, increasing the concentration of KCl enhances the Tyr FL in a manner similar to GdnHCl for the H3−H4 tetramer (Figure 3B) and the H2A−H2B dimer (data not shown). Second, the rise in FL at low [GdnHCl] is greatly attenuated in H3−H4 titrations performed in 0.2 M acrylamide, a nonionic quenching agent, without significantly altering the magnitude of FL change in the transition region between ∼1 and 2.5 M GdnHCl (data not shown). The third set of data supporting a local effect, rather than an unfolding transition, comes from stabilizing both histone oligomers with TMAO, trimethylamine-*N*-oxide. TMAO is a natural organic osmolyte that promotes preferential hydration of the native species and interacts unfavorably with the peptide backbone (*28*, *42*); TMAO is found in the urea-rich cells of coelacanths, sharks, and rays where it functions to stabilize proteins against the effects of urea. TMAO stabilization often has the effect of extending the native, pre-transition baseline region (i.e., ref *43* and the H2A−H2B data shown in this report).

Effect of TMAO on the Histone Oligomers. GdnHCl-induced unfolding transitions in 1 M TMAO were monitored by both CD and FL for the H2A−H2B dimer and the H3−H4 tetramer. Representative titrations are shown in Figure 4. For H2A−H2B, the pre-transition baselines extend

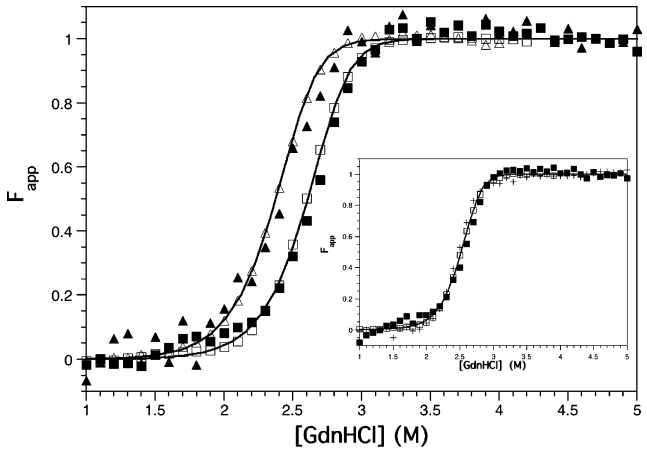

FIGURE 5: F_{app} curves for the equilibrium transitions of the H2A−H2B dimer in 1 M TMAO as a function of protein concentration. Data were collected by monitoring far-UV CD at 224 nm and Tyr FL at 305 nm at GdnHCl concentrations from 0 to 6 M; however, the transition regions have been expanded for clarity. The lines represent the global fits of the data to a two-state dimer unfolding model. Dimer concentrations: 0.5 μM (▲, CD 222 nm; △, Tyr FL) and 4.2 μM (■, CD 224 nm; □, Tyr FL). Inset: 2 μM data (■, CD 224 nm, unfolding; +, CD 224 nm, refolding; □, Tyr FL). Conditions are given in the legend of Figure 3.

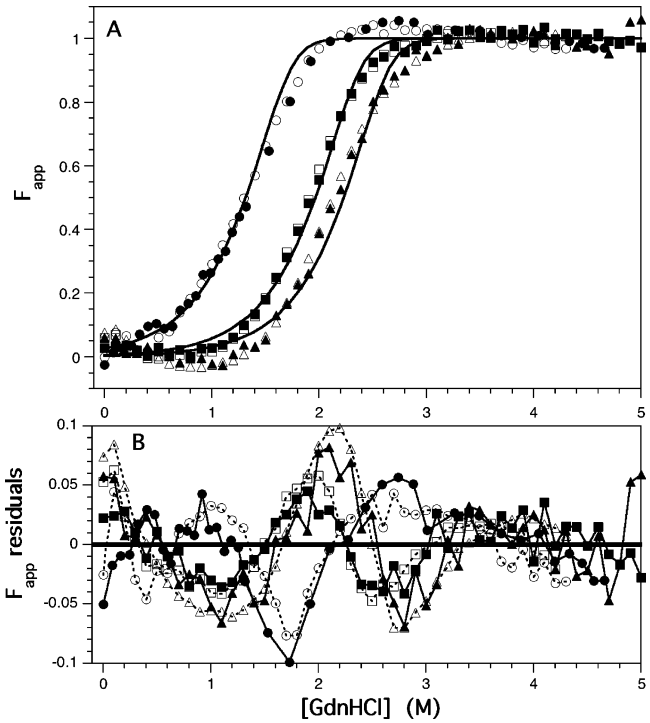

FIGURE 6: F_{app} curves for the equilibrium transitions of the H3−H4 tetramer in TMAO as a function of protein concentration. Data were collected by monitoring far-UV CD and Tyr FL as a function of [GdnHCl]. (A) Representative data fit to a two-state tetramer model. 0.25 μM tetramer CD (●) and FL (○); 2 μM tetramer CD (■) and FL (□); and 4.6 μM tetramer CD (▲) and FL (△). The lines represent the global fits of the data. (B) Residuals between data and the fits shown in panel A. Residuals for CD and FL data are shown as solid and dashed lines, respectively. Conditions: 1 M TMAO, 20 mM potassium phosphate, pH 7.2, 1 mM EDTA, 3 mM β-ME, 200 mM KCl, at 25 °C.

to ~2 M GdnHCl, further than in the absence of TMAO (Figure 4A). A sharp increase in FL is still observed between 0 and 1 M GdnHCl, followed by a linear region that was used as the native baseline in the global fitting of the data. The H3−H4 FL pre-transition baseline still exhibited curvature and lacked a distinctly linear region as seen for the more stable H2A−H2B dimer. Therefore, the H3−H4 pre-transition baselines were fit to a power function (legend of Figure 4). The unfolding transition of the tetramer is also shifted to higher [GdnHCl], most clearly seen in the CD data (Figure 4B).

The CD and FL data from several GdnHCl titrations in 1 M TMAO, over a range of oligomer concentrations, were globally fitted to two-state models. Data from different spectroscopic probes and at different oligomer concentrations are compared in the F_{app} curves shown in Figures 5 and 6. The data sets for the global fits also included refolding titrations (see Materials and Methods). The folding and unfolding titrations of both histone oligomers are in good agreement, demonstrating the high reversibility of the equilibria (i.e., Figure 5 inset). For H2A−H2B, the unfolding of tertiary and quaternary structures (detected by intrinsic Tyr FL) are coincident with the unfolding of secondary structures (detected by far-UV CD). This agreement supports the applicability of a two-state model for an unfolding equilibrium between folded dimer and unfolded monomers with no detectable, populated intermediates. The quality of the global fits of the data as a function of protein concentration is also an important determinant of the applicability of a two-state model. For the H2A−H2B dimer, the protein concentration dependence of the data set is well-described by a global fit to a dimeric, two-state equilibrium model in the absence and presence of TMAO (Figures 3 and 5). The parameters describing the stability of the H2A−H2B dimer in 1 M TMAO are given in Table 1.

For the H3−H4 system, the global fits to a two-state equilibria between folded tetramer and unfolded monomers, at different monomer concentrations, yielded modest agreement between the data and the model (Figure 6). The unfolding transitions monitored by CD and FL appeared to be coincident, in support of a two-state model. However, the two-state tetramer model could not adequately describe the protein concentration dependence of the titrations. A

Table 1: Parameters Describing the GdnHCl-Induced Equilibrium Unfolding Reactions of the H3−H4 Tetramer and the H2A−H2B Dimer in 1 M TMAO[a]

parameter	$(H3-H4)_2$ to 2 (H3−H4)	H3−H4 dimer to 2U monomers	H2A−H2B dimer to 2U monomers
$\Delta G°$ (H_2O) (kcal mol^{-1})	10 (1)	12.4 (0.6)	21.0 (0.9)
m value (kcal mol^{-1} M^{-1})	2.2 (0.6)	2.9 (0.3)	5.4 (0.3)
ΔG (kcal mol^{-1}) 10 μM monomer[b]	2.8	5.6	14.2
C_M (M GdnHCl) 10 μM monomer[b]	1.1	1.9	2.6

[a] Conditions: 1 M TMAO, 20 mM potassium phosphate, pH 7.2, 1 mM EDTA, 3 mM β-ME, and 200 mM KCl, at 25 °C. The values in parentheses are the error of one standard deviation from rigorous error analysis of the global fits of the data. $\Delta G°(H_2O)$ values are the free energy of unfolding at the standard state of 1 M oligomer. ΔG values are the free energy values in the absence of denaturant normalized to 10 μM monomer. [b] Monomer concentration of the stability curves shown in Figure 9. The C_M value is the [GdnHCl] that represents the midpoint of the given equilibrium at 10 μM monomer.

significantly better global fit, over all protein concentrations, was obtained when a two-state dimeric model was employed. The reduced χ^2 value for the fit to the dimer model was 30% of that for the tetramer model fit (same number of degrees of freedom and fitting parameters); the span of the residuals of the dimeric fit were also smaller, ±0.04 rather than ±0.1. The F_{app} curves for the CD and FL titrations in the two-state dimer fit were nearly coincident (data not shown). The global fits yielded $\Delta G°(H_2O)$ and m values of 11.8 kcal mol^{-1} and 2.6 kcal mol^{-1} M^{-1}. The comparison of the dimer and tetramer two-state fits demonstrate that the major transition reported by CD and FL is the dissociation and unfolding of the H3−H4 dimers. Clearly, the H3−H4 dimer is a significantly populated equilibrium intermediate in the unfolding of the H3−H4 tetramer.

Two observations suggested it might be possible to fit the data to a three-state model: (1) the poor quality of the tetrameric global fit of the protein concentration dependence over a concentration range of ~20-fold and (2) the low m value determined from the dimeric fits of the H3−H4 equilibrium data (2.6 kcal mol^{-1} M^{-1}) as compared to H2A−H2B (5.4 kcal mol^{-1} M^{-1}), a similarly sized protein complex. Similar types of data have indicated the presence of equilibrium intermediates in other protein folding studies that were apparently well-described by two-state models, such as *E. coli* factor for inversion stimulation (*44*) and *E. coli* RNAse H (*45*).

However, with CD and FL data alone, no reliable fits could be made to a three-state model with a dimeric intermediate. The data did not sufficiently deviate from a dimeric two-state model, either by divergence of the transitions monitored by different spectral probes or presence of multiple inflection points in the transition region. By far-UV CD, there is no detectable signal change between the folded H3−H4 dimers and the H3−H4 tetramer. The lack of change in far-UV CD was demonstrated previously by the lack of pH dependence of the CD spectra between pH 9 (predominantly tetramer) and pH 4 (predominantly dimer) in the studies by Moudrianakis et al. (*25*). This lack of far-UV CD sensitivity was confirmed by stopped-flow pH jumps from pH 5 to 7; no kinetics or detectable change were observed between the initial, pH 5 spectral signal and the final, post-jump, pH 7 signals. SF−FL pH jumps did not reveal any change in intrinsic Tyr FL between tetramer and dimer in the absence of GdnHCl; a small signal change may still exist at low GdnHCl concentrations.

HPLC−SEC chromatograms (Figure 2A) in 0 and 1 M TMAO suggested that the folded ensemble of H3−H4 was a mixture of tetrameric and dimeric species in the absence of stabilizing cosolute, but in 1 M TMAO, the native ensemble was predominantly tetrameric. This conclusion was supported by the kinetics of H3−H4 unfolding, which permitted direct quantitation, at a preset monomer concentration, of the amount of dimer and tetramer as a function of low [GdnHCl]. Stopped-flow CD and SF−FL unfolding jumps in the absence of TMAO were best described by two-exponentials, with the two kinetic phases having similar amplitudes. A representative SF−FL unfolding trace is shown in Figure 7A, described by relaxation times of 0.29 and 3.5 s. The dependence of the amplitudes on initial [GdnHCl] indicated the presence of two types of native species (Figure 7C), with the equilibrium shifting, with

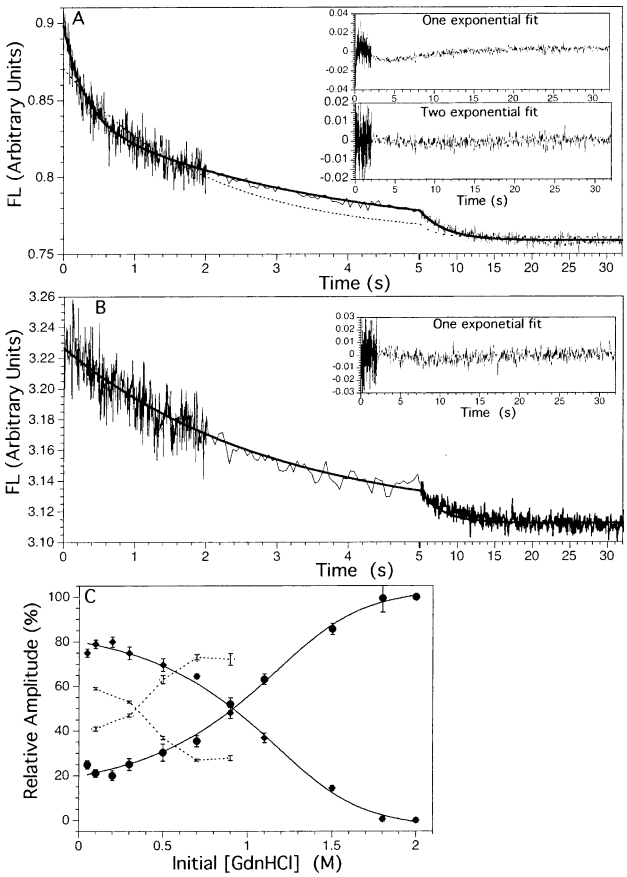

FIGURE 7: Stopped-flow FL unfolding kinetics for H3−H4 oligomer. (A) Kinetic trace for the unfolding to 2.5 M GdnHCl in the absence of TMAO. The thick solid line represents the fit to two exponentials; the dotted line represents the fit to one exponential. Shown in the inset are the residuals for fits to one and two exponentials. (B) Kinetic trace for the unfolding to 2.6 M GdnHCl in 1 M TMAO. The thick solid line represents the fit to a single exponential. The residuals for the fit are shown in the inset. (C) Relative amplitudes of the two SF−FL unfolding phases in 0 and 1 M TMAO (open and closed symbols, respectively). The amplitudes of the faster and slower unfolding phases are represented by circles and diamonds, respectively. The solid lines represent the results of the global fit of the 1 M TMAO data to a three-state model; the dotted lines are drawn to guide the eye for the 0 M TMAO amplitudes. The standard deviation of the amplitudes are shown (or are smaller than the symbol). Conditions: 1 μM tetramer, 20 mM potassium phosphate, pH 7.2, 1 mM EDTA, 3 mM β-ME, 200 mM KCl, at 25 °C.

increasing [GdnHCl], to favor the population of the faster unfolding, less structured (dimeric) species. In contrast, if the two kinetic phases arose because of the presence of a transiently populated unfolding intermediate, the relative amplitudes of the two phases should be independent of initial [GdnHCl]. The kinetic unfolding reactions in 1 M TMAO from 0 M GdnHCl (Figure 7B) could be much better described by a single exponential, with a relaxation time of 3.0 s, similar to the slower unfolding phase observed in the absence of TMAO. At higher initial [GdnHCl], the 1.0 M TMAO unfolding exhibited two exponential phases. Kinetic unfolding data in 1 M TMAO were collected as a function of initial [GdnHCl] and globally fitted to two exponentials with linked relaxation times (solid symbols, Figure 7C). The unfolding amplitudes report on the relative populations of tetramer and dimer at low [GdnHCl]; these data were added to the global fit of the CD and FL equilibrium data. This

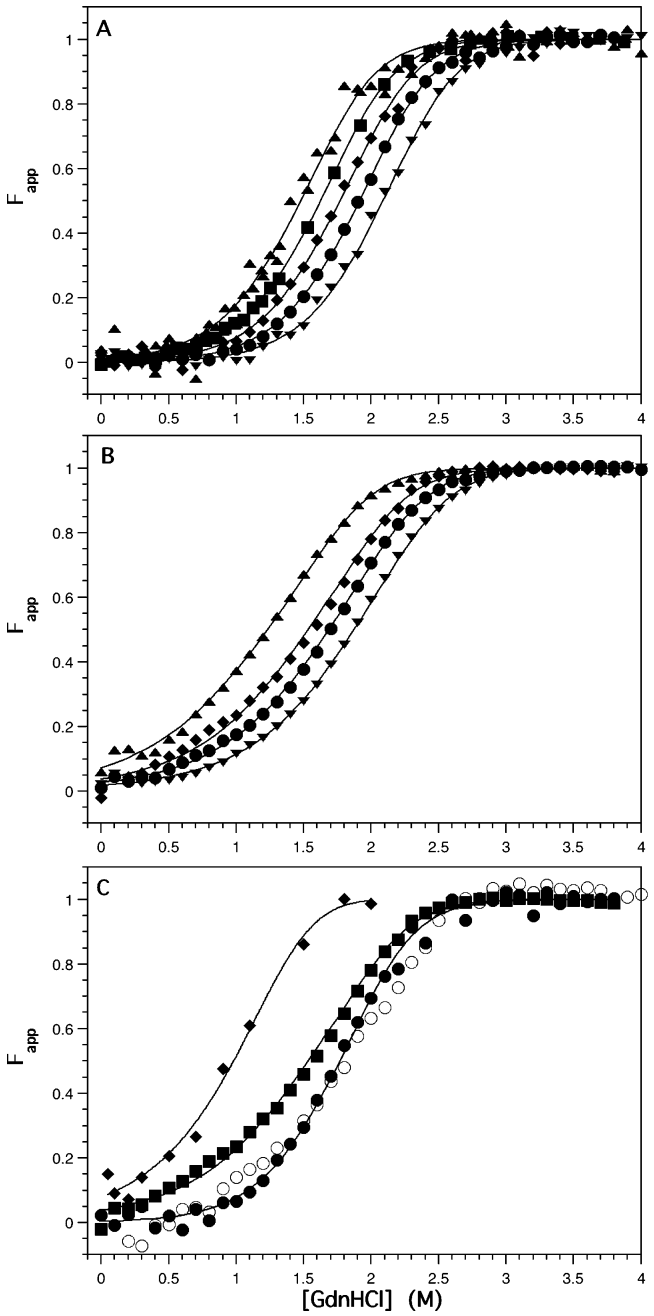

FIGURE 8: F_{app} curves for the equilibrium unfolding of the H3−H4 tetramer fitted to a three-state model between folded tetramer, two H3−H4 dimers, and four unfolded monomers. The lines represent the results of the global fits of the data. CD and FL data are shown in panels A and B, respectively. Tetramer concentrations: 0.25 μM, ▲; 0.5 μM, ■; 1 μM, ◆; 2 μM, ●; and 4.6 μM, ▼. (C) Comparison of data from different probes at 1 μM tetramer. Unfolding kinetic amplitudes, ◆; FL, ■; CD unfold, ●; and CD refold, ○. Conditions are given in legend of Figure 6.

additional information helped determine the parameters describing the equilibrium between H3−H4 tetramer and dimers.

This combined set of equilibrium and kinetic data were globally fitted to a three-state model with equilibria between tetramer and two dimers and between dimers and unfolded monomers. The results of the fits are shown in the F_{app} curves shown in Figure 8. The reduced χ^2 value of the three-state global fit demonstrated a statistically significant improvement relative to the two-state models and was 56 and 17% of those

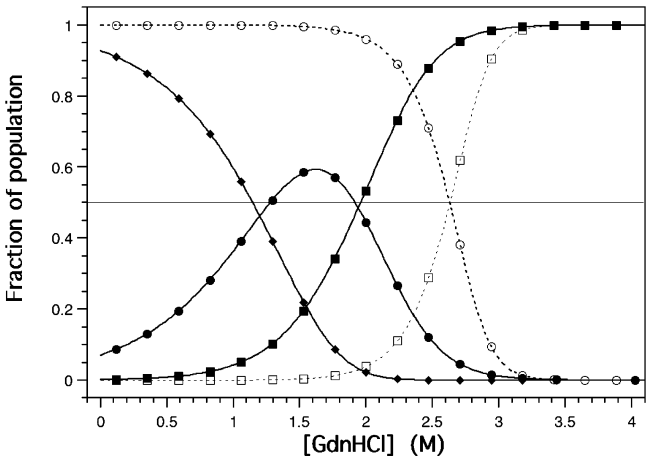

FIGURE 9: Stability curves of the histone oligomers at a concentration of 10 μM monomer in 1 M TMAO. H3−H4 curves are shown in solid lines and the H2A−H2B curves in dotted lines. H3−H4 tetramer, ◆; H3−H4 dimer, ●; unfolded H3 and H4 monomers, ■; H2A−H2B dimer, ○; and unfolded H2A and H2B monomers, □.

for the dimer and tetramer models, respectively. The three-state fit contained five additional parameters, relative to the two-state dimer model: $\Delta G°(H_2O)$ and m values for the tetramer−dimer equilibrium and Z values for the CD, FL, and kinetic amplitude data. The Z value describes the similarity in signal between the equilibrium intermediate (the H3−H4 dimers) and the unfolded species; thus, Z values generally range from 0 (a nativelike intermediate) to 1 (an unfolded-like intermediate). For all CD data, the Z values were fixed at 0 because of the demonstrated lack of change in signal between tetramer and dimer (see above). For the kinetic amplitude data, the Z values were fixed at 1 to force the data to only describe the equilibrium between tetramer and dimer. The Z value was fitted, as a linked parameter, for the FL titrations, to extract any small amount of change that might be obscured by the steepness of the apparent native baseline. In the final global fit, the FL data were described by a Z value of 0.30 ± 0.03, suggesting a FL decrease of ~30% upon tetramer dissociation. The $\Delta G°(H_2O)$ (at 1 M oligomer) and m values determined from the global fits are given in Table 1 for both equilibria in the three-state fit.

It is common to compare $\Delta G°(H_2O)$ values at a standard state of 1 M oligomer (i.e., Table 1). However, it is misleading to compare a tetramer and dimer at similar oligomer concentrations, where the monomer concentrations are different. Therefore, free energy values for the unfolding equilibria in the absence of denaturant are also provided at a standard state of 10 μM monomer (Table 1). The fitted values in Table 1 were also used to generate stability curves for the three oligomerization interfaces (H3−H3 in the tetramer, H3−H4 in the histone fold, and H2A−H2B in the histone fold). The populations of the native, intermediate, and unfolded species as a function of [GdnHCl] are shown in Figure 9.

To assess the effects of the highly charged N-terminal tails on the relative instability of the H3−H4 dimer, the stability of a tail-deleted construct of H3−H4 was also determined by GdnHCl-induced denaturation. The ΔN−H4 construct began at Lys20, and the ΔN−H3 construct began at His39. Data were collected by monitoring far-UV CD and globally fitted to a two-state dimeric model. This model was deemed

Table 2: Changes in Solvent Accessible Surface Area for the Histone Oligomers upon Subunit Association and Folding[a]

	total (Å^2)	nonpolar (Å^2)	%NP	polar (Å^2)	% P
		ΔASA between subunits			
H2A to H2B	5190 (20)	3950 (10)	76 (0.6)	1240 (30)	24 (0.5)
H3 to H4	5100 (100)	3780 (10)	74 (2)	1300 (100)	26 (2)
H3 to H3	1225	963	79	262	21
		ΔASA for folding			
H2A−H2B	16 830 (40)	12 180 (40)	72.3 (0.1)	4660 (1)	27.7 (0.1)
H3−H4 dimer	16 190 (70)	11 000 (60)	68 (1)	5200 (100)	32 (1)
H3−H4 tetramer	34 970	23 810	68	11160	32

[a] The Δ(accessible surface area, ASA) values were calculated as described in the Materials and Methods, using the coordinates of the histones in the X-ray structure of the core nucleosome (*12*). The values calculated for the subunit interfaces assumed no unfolding of the polypeptides upon dissociation. Where possible, the average ΔASA values are shown for the two different dimers present in the core nucleosome pdb file; in values in parentheses are the ±range from the average.

appropriate because of the findings discussed above for the full-length protein and the excellent description of the data as a function of protein concentration (comparable to the WT H3−H4 fits shown in Figure 8B). The $\Delta G°$ (H_2O) and *m* values of ΔN−H3/ΔN−H4 were 11.7 ± 0.3 kcal mol^{-1} and 2.6 ± 0.2 kcal mol^{-1} M^{-1}, similar to those determined for the full-length H3−H4 dimer when fit to the same model (see above).

Changes in Solvent Accessible Surface Area upon Folding and Association of the Histone Oligomers. To elucidate the reasons for the differences in the observed $\Delta G°$(H_2O) and *m* values for the histone oligomers, the changes in solvent accessible surface area (ΔASA) were calculated for assembly of the oligomeric interfaces and between the native and the unfolded species. The results are summarized in Table 2. The values of ΔASA are dissected into polar and nonpolar components. The ASA values for the folded proteins were determined using the coordinates of the histones in the context of the core nucleosome (*12*). A caveat to the interpretation of these calculated ASA values is the assumption that the structures of the histone oligomers are similar free in solution and in the context of the nucleosome. This is a reasonable assumption at the level of limited detail employed here, assessing what residues are on the surface, and solvent accessible, and what residues are significantly buried from solvent in the protein structure.

In nucleosome X-ray crystal structures, the tails of the eight histones are not completely resolved. Calculations were also made on truncated model structures, in which the coordinates for regions in an extended conformation were not included. The regions used in these calculations were H2A, residues 16−109; H2B, residues 32 to C-terminus; H3, residues 41 to C-terminus; and H4, residues 20 to C-terminus. The results obtained for the truncated structures were very similar to those reported in Table 2; there was a minor decrease in ΔASA but no change in the percentages of polar and nonpolar surface area.

DISCUSSION

In the absence of TMAO, the oligomeric state of the H3−H4 histones appears to be an equilibrium between H3−H4 dimers and $(H3−H4)_2$ tetramer. The folded baselines in GdnHCl-induced denaturation studies were too poorly defined to permit a unique, meaningful fit of the data. Therefore, the stability of the histone oligomers were examined in the presence of 1 M TMAO. TMAO had the effect of extending the native baselines of GdnHCl titrations and enhancing the tetrameric state of the H3−H4 ensemble. For comparison, 1 M TMAO stabilized the H2A−H2B dimer by 4 kcal mol^{-1}. GdnHCl denaturation in the presence of 1 M TMAO permits a direct thermodynamic comparison of the stability of the histone oligomers and their interfaces at pH and temperature values that are comparable to physiological conditions. The denaturation transitions of the H2A−H2B dimer were well-described by a two-state equilibrium model between folded dimer and two unfolded monomers. However, the H3−H4 ensemble was best described by a three-state model, with a folded, H3−H4 dimeric intermediate. The H3−H4 data allows comparisons in stability to be made between two types of dimerization interfaces, the H3−H3 four-helix bundle and the H3−H4 histone fold.

Stability of the H3−H3 Tetramer Interface. Association constants for the equilibrium between the $(H3−H4)_2$ tetramer and the H3−H4 dimer have been reported for a series of ionic conditions (*40*). The free energies calculated from these K_a values at moderate ionic strengths (comparable to this report) are 7−8 kcal mol^{-1}. These stabilities are comparable to the $\Delta G°$(H_2O) value measured by GdnHCl denaturation, 10 kcal mol^{-1}. The enhanced stability measured by denaturation probably arises from the stabilizing presence of 1.0 M TMAO.

When compared at a standard state of 1 M oligomer, the least stable interface in the isolated core histones (as opposed to the histone octamer) is that of the H3−H3 four-helix bundle that forms the tetramer interface. This instability is even more striking when the free energies are normalized to the same monomer concentration, at more physiological concentrations, such as 10 μM monomer (Table 1). Similarly, comparing the C_M values (Table 1), it takes nearly twice the [GdnHCl] to dissociate the H3−H4 histone fold as compared to the H3−H3 four helix bundle. The ΔASA calculations demonstrate that the surface area exposed upon disruption of the four-helix bundle interface is predominantly hydrophobic (Table 2). In fact, the hydrophobicity of the tetramer interface is slightly greater than the interface buried in the histone fold dimerization motif of either the H2A−H2B or the H3−H4 dimer. The relative instability of the H3−H3 interface can be explained by its comparatively small surface area, ∼24% of the surface area buried in the histone fold.

Why Is the H3−H4 Dimer Less Stable than the H2A−H2B Dimer? The stability of the two heterotypic dimers present in the core nucleosome can be directly compared in two ways: the $\Delta G°$(H_2O) and the C_M values.

By either parameter, the H3−H4 dimer is significantly less stable than the H2A−H2B dimer, despite the high conservation of the structure of their folds.

Several structural comparisons were made to elucidate the reason for the differences in stability of the histone fold motifs. (1) The N-terminal tails of the histone dimers are not the cause of the differences in stability. A ΔN−H3/ΔN−H4 construct, which removes all of the sequences that are poorly structured in the nucleosome X-ray structure (*12*), exhibits values of $\Delta G°(H_2O)$ and *m* that are similar to those of the full-length recombinant dimer. The subtle effects of N-terminal tail deletions on the H2A−H2B dimer are discussed elsewhere (*46*). (2) The helical propensity of the four histone sequences were estimated using the program AGADIR (*47*), and no significant differences were found to explain the stability differences. (3) The ΔASA values for dissociation of the H2A−H2B and H3−H4 histone fold interfaces are similar in size and composition (Table 2). (4) The ΔASA upon unfolding are slightly greater in size and more hydrophobic in composition for the H2A−H2B dimer, relative to the H3−H4 dimers (Table 2). These global differences cannot explain the large stability differences but suggest that the details of the burial of polar residues may be informative. (5) The solvent exposure of residues that are expected to be charged at pH 7.2 were examined for each histone dimer. There is a significant difference in the solvent accessibility of charged residues present in H2A−H2B and H3−H4, and burial of charged residues can be destabilizing to proteins (see below).

The average solvent accessible surface areas for the charged atoms of Asp, Glu, and Arg residues are significantly greater for H2A−H2B (24, 22, and 38 Å^2, respectively) than for H3−H4 (17, 15, and 30 Å^2, respectively). A similar but smaller difference is also observed in comparison of Lys residues, 64 and 61 Å^2 for H2A−H2B and H3−H4, respectively. The differences in burial of charged residues are more striking when individual residues are examined. For many of the side chain polar atoms, solvent exclusion near the protein surface is the result of the formation of hydrogen bonds or salt bridges that sterically hinder solvent access. Residues were considered to be buried only if three criteria were met: (1) the ionizable atom in the side chain had ASA values that were less than 10% of that observed in a maximally extended, solvated side chain. This low cutoff was used to distinguish between atoms occluded near the protein surface and those that are interior to the protein (*48*); (2) the low ASA value was observed in both structures of the residue in the nucleosome; and (3) if two ionizable atoms were present in the side chain (i.e., Oδ1 and Oδ2 of Asp, Oϵ1 and Oϵ2 of Glu, and Nη1 and Nη2 of Arg), both atoms had <10% ASA in both polypeptides represented in the nucleosome. This latter criteria eliminated many residues in which one atom was buried in the protein surface but the other atom was solvent exposed. By these criteria, H2A−H2B had no buried charged residues, and no Lys residues were buried in either histone fold. However, five charged residues were found to be buried in the H3−H4 dimer: Glu97, Arg116, Asp123, and Glu133 in H3 and Asp85 in H4 (*Xenopus laevis* numbering).

The buried H3−H4 residues are in environments containing several hydrophobic groups; however, polar contacts can be identified for each buried residue. The H3 residues Asp123 and Arg116 form a buried salt bridge; Asp123 is also within hydrogen bond distance of the backbone N of H3−Met120 and perhaps that of H3−Ala111. H3−Glu97 forms two hydrogen bonds to the backbone nitrogens of Leu61 and Ile62. H3−Glu133 forms hydrogen bonds with the side chains of H3−Arg128 and H3−Tyr99 and a partially buried salt bridge with H3−Arg131. H4−Asp85 forms a partially buried salt-bridge with H4−Arg78.

All of the buried charged residues are highly conserved, based on the alignments of ∼100 H3 and H4 sequences (*49*). H3-Glu97 is completely conserved. H3−Arg116 is conservatively substituted with Lys in the sequence of *Asellus aquaticus* (6686555) and is replaced by a Cys in two mouse H3 variants. This residue was identified as a SIN mutation, which relieved the need for the SWI/SNF chromatin remodeling complex in yeast (*50*). The interacting residue in the buried salt bridge, H3−Asp123, is conservatively substituted with Glu and Asn in H3 variants from *Homo sapiens* and *Caenorhabditis elegans*. Only a Gly substitution in the *Asellus aquaticus* sequence does not conserve the polarity of the H3−123 residue, but this substitution appears to eliminate the compensating charge to the buried Lys in that Caenorhabditis sequence. H3−Glu133 is at the C-terminus of the four helix bundle tetramer interface and is conserved in ∼94% of the sequences that include this residue. H4−Asp85 is conserved in all but one *H. sapiens* sequence, where it is substituted by Ala. Therefore, in the vast majority of H3 and H4 sequences, the presence of buried salt bridges or charged hydrogen bonds are conserved. As these charged atoms are highly buried in the protein structure, they are not available to form interactions with DNA or other nucleosome-associated proteins. Therefore, their high degree of conservation is unlikely to arise from required interactions with other macromolecules in the cell. It is speculated that selection for the conservation of these buried charged residues may be because of their effects on the structural stability of the H3−H4 histone fold.

While this is still a controversial issue, there are a significant number of examples in which the burial of a salt-bridge or charged hydrogen bonds are destabilizing to a protein (*51*). Electrostatic calculations have estimated the free energy penalty for the burial of a salt bridge to be in the range of 2.5−5 kcal mol^{-1} (*52*). The free energy penalty for burial of a single charged residue that forms hydrogen bonds was ∼4.2 kcal mol^{-1}. Mutational studies have shown that removal of a buried salt bridge in dimeric *Arc* repressor can stabilize the protein by 2−4.5 kcal mol^{-1}, depending on the isosteric similarity between the wild-type and the mutated residue (*53*). Burial of single charged residues have been shown to destabilize proteins by 2−7 kcal mol^{-1}, the variation arising from the degree of hydrogen bond formation (*54*−*57*). Using the most modest estimates of destabilization for the partial to complete burial of three salt bridges and burial of a charged hydrogen, the predicted destabilization of H3−H4 is ∼8 kcal mol^{-1}. This value is very similar to the free energy difference between the H3−H4 dimer and the H2A−H2B dimer, which does not contain buried charged residues (Table 1).

Interpretation of the m Values Determined from GdnHCl Denaturation Studies. The *m* value determined from chemical denaturation is empirically the dependence of the unfolding

transition on denaturant concentration. The fitted *m* values for the unfolding of the H3−H4 dimer are lower than those of the H2A−H2B dimer. This difference can be explained by a coupling between the two equilibria in the unfolding of the H3−H4 ensemble (dissociation of the tetramer, four-helix-bundle interface, and unfolding of the two H3−H4 dimers to four unfolded monomers).

Generally, the *m* value, in a two-state system, reflects the changes in solvent accessible surface area between the native and the unfolded species (ΔASA) (*39*); indeed, there is a strong correlation between measured *m* values and ΔASA. The ΔASA calculations of the H2A−H2B based on the nucleosome structure (Table 2) predict *m* values of 4.8−4.6 kcal mol^{-1} M^{-1} with and without the N- and C-terminal tails, respectively. The experimentally determined *m* values of the dimer, 6.4 to 5.4 kcal $mol^{-1}M^{-1}$ in the absence and presence of TMAO, respectively, are significantly higher than these estimates. Therefore, the H2A−H2B tails, in the absence of DNA, must adopt partially folded, solvent excluding structures. A similar conclusion was drawn from urea-unfolding equilibrium experiments on H2A−H2B (*29*). For globular proteins, there is also a strong correlation between number of residues and ΔASA values upon folding (*39*); the correlation permits an estimate of the *m* value based on number of residues, when a structure is not known, such as that of the N-terminal tails in the absence of DNA. For a protein of 251 residues, such as H2A−H2B, the expected *m* value would be ∼6 kcal mol^{-1} M^{-1}, in excellent agreement with the *m* value observed in 0 M TMAO, 6.4 kcal mol^{-1} M^{-1}.

The decreased *m* value of H2A−H2B in 1 M TMAO, 5.4 kcal mol^{-1} M^{-1}, does not appear to arise from the presence of an equilibrium intermediate; the H2A−H2B unfolding is well-described by a dimeric two-state model on the basis of the coincidence of far-UV CD and Tyr FL data and the quality of the global fit at all protein concentrations (Figure 5). The effect of TMAO on the *m* value of the H2A−H2B dimer is most likely explained by a difference in ΔASA between the folded and the unfolded ensembles populated in 0 and 1 M TMAO. TMAO promotes the exclusion of surface area, especially main chain surface area, from solvent access in most proteins, thus destabilizing the unfolded state (*58*). Therefore, it is likely that, in 1 M TMAO, the unfolded state of the H2A and H2B monomers excludes more solvent than their unfolded structures in the absence of TMAO.

Comparison to Previous Studies. The data in this report demonstrate that the H3−H4 tetramer and dimers unfold at lower denaturant concentrations than the H2A−H2B dimer and therefore are less stable (Figures 3, 4, and 9). The relative instability of the H3−H4 tetramer is in contrast to earlier work from the Isenberg lab (*22*, *23*). This difference is the result of the different denaturation/disassembly methods used, and thus, the relative unfolded/unassembled states. The data in this report measures the stability between unfolded dissociated monomers, as might exist in the cell, and assembled histone oligomers. The Isenberg studies measured the free energy difference between homotypic and heterotypic assemblies.

The thermal denaturation results of the Moudrianakis lab demonstrated that the H3−H4 dimer is more thermally stable than the H2A−H2B dimer (*25*). Direct comparisons between the two dimeric systems could only be made at ∼pH 5; however, similar conclusions are drawn if the stability of the H2A−H2B dimer at pH 7.5 is compared to the H3−H4 dimer at pH 5. When the free energy of unfolding of a protein is extrapolated to physiological temperatures, an accurate determination of the ΔC_p value is essential. From differential scanning calorimetry data near pH 5 (*24*, *25*), the free energy of unfolding of the H3−H4 dimer is only 0−1.2 kcal mol^{-1} greater than that of H2A−H2B, in the physiological temperature range of 20−40 °C. However, the certainty of this extrapolation is unclear because of the unusually low values of ΔC_p for the H3−H4 dimer. Like the *m* value in chemical denaturation, in a two-state equilibrium system, there is a strong correlation between ΔC_p and the ΔASA (*39*). The expected ΔC_p values for the histone dimers, based on the ΔASA values given in Table 2, are 3.1−3.2 kcal mol^{-1} K^{-1}. The values for the H2A−H2B dimer were generally close to these predicted values, 2.6−3.0 kcal mol-$dimer^{-1}$ K^{-1}; however, the ΔC_p value at pH 5.5 is significantly less, 1.8 kcal mol-$dimer^{-1}$ K^{-1} (*24*). The H3−H4 ΔC_p values are much lower than predicted, 1.0−1.4 kcal mol-$dimer^{-1}$ K^{-1}. These low ΔC_p values were attributed to a higher than usual heat capacity of the native H3−H4 dimer (*25*), which was explained by an unusually high apolar accessible surface area. However, this explanation is inconsistent with the ASA values measured in the current study. The absolute values of nonpolar accessible surface area of the folded histone dimers are similar, as are the percentages of nonpolar ASA, 51 and 55% for H2A−H2B and H3−H4 dimers, respectively. Measured ΔC_p values can be lower than expected because of protein aggregation or limited oligomerization, a common problem with H3−H4 complexes (*26*, *40*), and/or the presence of an intermediate, even when the data is apparently well-described by a two-state mechanism (i.e., refs *44* and *45*). If a ΔC_p of the magnitude expected for H3−H4 dimer (and observed for H2A−H2B dimers) is used in the extrapolation of the stability to physiological temperatures, the H3−H4 dimer has less than half the stability of the H2A−H2B dimer.

Implications on the Function of the Nucleosome. In eukaryotes, DNA is complexed with histone proteins to form the nucleosome. The nucleosome is a dynamic structure of fundamental importance in DNA packaging and other DNA-based chemistries in the cell, including transcription, replication, and repair (*59*, *60*). While the subject of intense study for many years (i.e., refs *19* and *23*), the description of the thermodynamics and kinetics of nucleosome assembly and unfolding is not complete. Understanding the stability of the histone oligomers is an important beginning for a biophysical, molecular description of the nucleosome and the dynamic features that allow this structure to modulate DNA chemistries in the cell.

In the cell, the H3−H4 tetramer is almost constitutively associated with DNA, while the H2A−H2B dimer can dissociate from and exchange between nucleosomes (*19*, *23*). It is interesting that the tetramer is significantly less stable than the dimer. The marginal stability of the tetramer may make it a more malleable, plastic structure that can be manipulated by the proteins that bind to the nucleosome and enzyme complexes that: (1) modulate chromatin structure, such as the ATP-dependent chromatin remodeling complexes or (2) interact with the DNA template, such as RNA and DNA polymerases. The binding of the tetramer to positively

and negatively super-coiled DNA demonstrates the necessity of a malleable tetramer structure, particularly in the H3−H3 interface (*61*). The conformational flexibility postulated to explain the ability of the tetramer to bind to the differently supercoiled DNA is supported by the fragile nature of the H3−H3 interface quantified in this report. In contrast, the more stable H2A−H2B dimer is removed from DNA during certain cellular processes. For example, transcriptionally active chromatin is often deficient in H2A−H2B dimers (*62*, *63*). It is speculated that the function of H3−H4 may require it to be unstable, and this instability has evolved by the conservation of buried charged side chains.

ACKNOWLEDGMENT

We are grateful to Brandon J. Placek for providing some of the H2A−H2B dimer used in this study and to Traci Topping for critical review of the manuscript. The pET overexpression vectors were kindly provided by Karolin Luger and Timothy Richmond of the Institute for Molecular Biology and Biophysics at the ETHZ, Zurich, Switzerland (K. Luger currently at Colorado State University).

REFERENCES

1. Shortle, D. (1999) Structure prediction: The state of the art, *Curr. Biol. 9*, R205−9.
2. Bonneau, R., and Baker, D. (2001) Ab initio protein structure prediction: progress and prospects, *Annu. Rev. Biophys. Biomol. Struct. 30*, 173−89.
3. Gunasekaran, K., Eyles, S. J., Hagler, A. T., and Gierasch, L. M. (2001) Keeping it in the family: folding studies of related proteins, *Curr. Opin. Struct. Biol. 11*, 83−93.
4. Kim, D. H., Jang, D. S., Nam, G. H., and Choi, K. Y. (2001) Folding mechanism of ketosteroid isomerase from *Comamonas testosteroni*, *Biochemistry 40*, 5011−7.
5. Kim, D. H., Nam, G. H., Jang, D. S., Yun, S., Choi, G., Lee, H. C., and Choi, K. Y. (2001) Roles of dimerization in folding and stability of ketosteroid isomerase from *Pseudomonas putida* biotype B, *Protein Sci. 10*, 741−52.
6. Wallace, L. A., Sluis-Cremer, N., and Dirr, H. W. (1998) Equilibrium and kinetic unfolding properties of dimeric human glutathione transferase A1−1, *Biochemistry 37*, 5320−8.
7. Wallace, L. A., and Dirr, H. W. (1999) Folding and assembly of dimeric human glutathione transferase A1-1, *Biochemistry 38*, 16686−94.
8. Hornby, J. A., Luo, J. K., Stevens, J. M., Wallace, L. A., Kaplan, W., Armstrong, R. N., and Dirr, H. W. (2000) Equilibrium folding of dimeric class mu glutathione transferases involves a stable monomeric intermediate, *Biochemistry 39*, 12336−44.
9. McCallister, E. L., Alm, E., and Baker, D. (2000) Critical role of *β*-hairpin formation in protein G folding, *Nat. Struct. Biol. 7*, 669−73.
10. Kim, D. E., Fisher, C., and Baker, D. (2000) A breakdown of symmetry in the folding transition state of protein L, *J. Mol. Biol. 298*, 971−84.
11. Ferguson, N., Capaldi, A. P., James, R., Kleanthous, C., and Radford, S. E. (1999) Rapid folding with and without populated intermediates in the homologous four-helix proteins Im7 and Im9, *J. Mol. Biol. 286*, 1597−608.
12. Luger, K., Mader, A. W., Richmond, R. K., Sargent, D. F., and Richmond, T. J. (1997) Crystal structure of the nucleosome core particle at 2.8 Å resolution, *Nature 389*, 251−60.
13. Arents, G., Burlingame, R. W., Wang, B. C., Love, W. E., and Moudrianakis, E. N. (1991) The nucleosomal core histone octamer at 3.1 Å resolution: a tripartite protein assembly and a left-handed superhelix, *Proc. Natl. Acad. Sci. U.S.A. 88*, 10148−52.
14. Arents, G., and Moudrianakis, E. N. (1995) The histone fold: A ubiquitous architectural motif utilized in DNA compaction and protein dimerization, *Proc. Natl. Acad. Sci. U.S.A. 92*, 11170−74.
15. Baxevanis, A. D., Arents, G., Moudrianakis, E. N., and Landsman, D. (1995) A variety of DNA-binding and multimeric proteins contain the histone fold motif, *Nucleic Acids Res. 23*, 2685−91.
16. Baxevanis, A. D., and Landsman, D. (1998) Histone sequence database: new histone fold family members, *Nucleic Acids Res. 26*, 372−75.
17. Xie, X., Kokubo, T., Cohen, S. L., Mirza, U., Hoffmann, A., Chait, B. T., Roeder, R. G., Nakatani, Y., and Burley, S. K. (1996) Structural similarity between TAFs and the heterotetrameric core of the histone octamer, *Nature 380*, 316−22.
18. Birck, C., Poch, O., Romier, C., Ruff, M., Mengus, G., Lavigne, A. C., Davidson, I., and Moras, D. (1998) Human $TAF_{II}28$ and $TAF_{II}18$ interact through a histone fold encoded by atypical evolutionary conserved motifs also found in the SPT3 family, *Cell 94*, 239−49.
19. Wolffe, A. R. (1998) *Chromatin: Structure and Function*, 3rd ed., Academic Press, San Diego, CA.
20. Cheung, P., Allis, C. D., and Sassone-Corsi, P. (2000) Signaling to chromatin through histone modifications, *Cell 103*, 263−71.
21. Isenberg, I. (1979) Histones, *Annu. Rev. Biochem. 48*, 159−91.
22. D'Anna, J. A., and Isenberg, I. (1974) A histone cross-complexing pattern, *Biochemistry 13*, 4992−97.
23. van Holde, K. (1989) *Chromatin*, Springer-Verlag, New York.
24. Karantza, V., Baxevanis, A. D., Freire, E., and Moudrianakis, E. N. (1995) Thermodynamic studies of the core histones: Ionic strength and pH dependence of H2A−H2B dimer stability, *Biochemistry 34*, 5988−96.
25. Karantza, V., Freire, E., and Moudrianakis, E. N. (1996) Thermodynamic studies of the core histones: pH and ionic strength effects on the stability of the $(H3-H4)/(H3-H4)_2$ system, *Biochemistry 35*, 2037−46.
26. Karantza, V., Freire, E., and Moudrianakis, E. N. (2001) Thermodynamic studies of the core histones: Stability of the octamer subunits is not altered by removal of their terminal domains, *Biochemistry 40*, 13114−123.
27. Luger, K., Rechsteiner, T. J., Flaus, A. J., Waye, M. M., and Richmond, T. J. (1997) Characterization of nucleosome core particles containing histone proteins made in bacteria, *J. Mol. Biol. 272*, 301−11.
28. Wang, A., and Bolen, D. W. (1997) A naturally occurring protective system in urea-rich cells: mechanism of osmolyte protection of proteins against urea denaturation, *Biochemistry 36*, 9101−8.
29. Gloss, L. M., and Placek, B. J. (2002) The Effect of Salts on the Stability of the H2A−H2B Histone Dimer, *Biochemistry 41*, 14951−59.
30. Gill, S. C., and von Hippel, P. H. (1989) Calculation of protein extinction coefficients from amino acid sequence data, *Anal. Biochem. 182*, 319−26.
31. Henry, E. R., and Hofrichter, J. (1992) Singular value decomposition: Application of analysis of experimental data, *Methods Enzymol. 210*, 129−92.
32. Zitzewitz, J. A., Bilsel, O., Luo, J., Jones, B. E., and Matthews, C. R. (1995) Probing the folding mechanism of a leucine zipper peptide by stopped-flow circular dichroism spectroscopy, *Biochemistry 34*, 12812−19.
33. Gualfetti, P. J., Iwakura, M., Lee, J. C., Kihara, H., Bilsel, O., Zitzewitz, J. A., and Matthews, C. R. (1999) Apparent radii of the native, stable intermediates and unfolded conformers of the α-subunit of tryptophan synthase from *Escherichia coli*, a TIM barrel protein, *Biochemistry 38*, 13367−78.
34. Gualfetti, P. J., Bilsel, O., and Matthews, C. R. (1999) The progressive development of structure and stability during the equilibrium folding of the alpha subunit of tryptophan synthase from *Escherichia coli*, *Protein Sci. 8*, 1623−35.
35. Beechem, J. M. (1992) Global analysis of biochemical and biophysical data, *Methods Enzymol. 210*, 37−54.
36. Pace, C. N. (1986) Determination and analysis of urea and guanidine hydrochloride denaturation curves, *Methods Enzymol. 131*, 266−80.
37. Santoro, M. M., and Bolen, D. W. (1992) A test of the linear extrapolation of unfolding free energy changes over an extended denaturant concentration range, *Biochemistry 31*, 4901−7.

38. Lee, B., and Richards, F. M. (1971) The interpretation of protein structures: Estimation of static accessibility, *J. Mol. Biol. 55*, 379−400.
39. Myers, J. K., Pace, C. N., and Scholtz, J. M. (1995) Denaturant *m* values and heat capacity changes: Relation to changes in accessble surface areas of protein folding, *Protein Sci. 4*, 2138−48.
40. Baxevanis, A. D., Godfrey, J. E., and Moudrianakis, E. N. (1991) Associative behavior of the histone $(H3-H4)_2$ tetramer: Dependence on ionic environment, *Biochemistry 30*, 8817−23.
41. Thomas, J. O. (1989) Chemical cross-linking of histones, *Methods Enzymol. 170*, 549−71.
42. Bolen, D. W. (2001) Protein stabilization by naturally occurring osmolytes, *Methods Mol. Biol. 168*, 17−36.
43. Henkels, C. H., Kurz, J. C., Fierke, C. A., and Oas, T. G. (2001) Linked folding and anion binding of the *Bacillus subtilis* ribonuclease P protein, *Biochemistry 40*, 2777−89.
44. Hobart, S. A., Meinhold, D. W., Osuna, R., and Colon, W. (2002) From two-state to three-state: The effect of the P61A mutation on the dynamics and stability of the Factor for Inversion Stimulation in an altered equilibrium denaturation mechanism, *Biochemistry 41*, 13744−54.
45. Spudich, G., and Marqusee, S. (2000) A change in the apparent *m* value reveals a populated intermediate under equilibrium conditions in *Escherichia coli* ribonuclease HI, *Biochemistry 39*, 11677−83.
46. Placek, B. J., and Gloss, L. M. (2002) The N-terminal Tails of the H2A−H2B Histones Affect Dimer Structure and Stability, *Biochemistry 41*, 14960−68.
47. Munoz, V., and Serrano, L. (1997) Development of the multiple sequence approximation within the AGADIR model of α-helix formation: comparison with Zimm−Bragg and Lifson−Roig formalisms, *Biopolymers 41*, 495−509.
48. Janin, J., Miller, S., and Chothia, C. (1988) Surface, subunit interfaces, and interior of oligomeric proteins, *J. Mol. Biol. 204*, 155−64.
49. Sullivan, S., Sink, D. W., Trout, K. L., Makalowska, I., Taylor, P. M., Baxevanis, A. D., and Landsman, D. (2002) The Histone Database, *Nucleic Acids Res. 30*, 341−2.
50. Kruger, W., Peterson, C. L., Sil, A., Coburn, C., Arents, G., Moudrianakis, E. N., and Herskowitz, I. (1995) Amino acid substitutions in the structured domains of histones H3 and H4 partially relieve the requirement of the yeast SWI/SNF complex for transcription, *Genes Dev. 9*, 2770−9.
51. Kumar, S., and Nussinov, R. (1999) Salt bridge stability in monomeric proteins, *J. Mol. Biol. 293*, 1241−55.
52. Hendsch, Z. S., and Tidor, B. (1994) Do salt bridges stabilize proteins? A continuum electrostatic analysis, *Protein Sci. 3*, 211−26.
53. Waldburger, C. D., Schildbach, J. F., and Sauer, R. T. (1995) Are buried salt bridges important for protein stability and conformational specificity? *Nat. Struct. Biol. 2*, 122−8.
54. Dao-pin, S., Anderson, D. E., Baase, W. A., Dahlquist, F. W., and Matthews, B. W. (1991) Structural and thermodynamic consequences of burying a charged residue within the hydrophobic core of T4 lysozyme, *Biochemistry 30*, 11521−9.
55. Stites, W. E., Gittis, A. G., Lattman, E. E., and Shortle, D. (1991) In a staphylococcal nuclease mutant the side-chain of a lysine replacing valine 66 is fully buried in the hydrophobic core, *J. Mol. Biol. 221*, 7−14.
56. Shao, X., Hensley, P., and Matthews, C. R. (1997) Construction and characterization of monomeric tryptophan repressor: a model for an early intermediate in the folding of a dimeric protein, *Biochemistry 36*, 9941−49.
57. Takano, K., Tsuchimori, K., Yamagata, Y., and Yutani, K. (2000) Contribution of salt bridges near the surface of a protein to the conformational stability, *Biochemistry 39*, 12375−81.
58. Bolen, D. W., and Baskakov, I. V. (2001) The osmophobic effect: Natural selection of a thermodynamic force in protein folding, *J. Mol. Biol. 310*, 955−63.
59. Wolffe, A., and Kurumizaka, H. (1998) The nucleosome: A powerful regulator of transcription, *Prog. Nucl. Acid Res. Mol. Biol. 61*, 379−422.
60. Workman, J. L., and Kingston, R. E. (1998) Alteration of nucleosome structure as a mechanism of transcriptional regulation, *Annu. Rev. Biochem. 67*, 545−79.
61. Hamiche, A., and Richard-Foy, H. (1998) The switch in the helical handedness of the histone (H3−H4)2 tetramer within a nucleoprotein particle requires a reorientation of the H3−H3 interface, *J. Biol. Chem. 273*, 9261−9.
62. Louters, L., and Chalkley, R. (1985) Exchange of histones H1, H2A, and H2B in vivo, *Biochemistry 24*, 3080−5.
63. Jackson, V. (1990) In vivo studies on the dynamics of histone−DNA interaction: evidence for nucleosome dissolution during replication and transcription and a low level of dissolution independent of both, *Biochemistry 29*, 719−31.
64. Kraulis, P. J. (1991) MOLSCRIPT: a program to produce both detailed and schematic plots of protein structures, *J. Appl. Crystallogr. 24*, 946−50.

BI026957R